Intermodulation Mechanism and Linearization of AlGaAs/GaAs HBT's

Joonwoo Lee, *Member, IEEE,* Woonyun Kim, *Student Member, IEEE,* Youngsik Kim, *Student Member, IEEE,* Taemoon Rho, *Member, IEEE,* and Bumman Kim, *Senior Member, IEEE*

***Abstract*—The intermodulation (IM) mechanism of heterojunction bipolar transistors (HBT's) has been studied by using an analytical nonlinear equivalent circuit model and Volterra-series analysis of the model. Although the third-order IM intercept point (IP3) does not depend on the emitter parameter, it is appreciably affected by base and collector parameters and has been substantially improved by utilizing punchthrough collector structure. The measured IP3 of punchthrough collector HBT's is 31 dBm with 150-mW dc power, which is higher than that of normal collector HBT's by 3 dB. The investigation of the cancellation effects of nonlinear elements reveals that the output nonlinear current components generated by emitter–base current source and base–collector current source cancel each other almost exactly, resulting in high linear characteristics of HBT's.**

***Index Terms*— Heterojunction bipolar transistors, intermodulation distortion, nonlinear distortion, semiconductor device modeling, Volterra series.**

I. Introduction

AlGaAs/GaAs heterojunction bipolar transistors (HBT's) are known for their low-distortion characteristics in linear power applications. Third-order intermodulation (IM) intercept points (IP3) as high as 33 dBm have been reported with 150-mW dc power [1], [2]. An internally matched linear-power HBT with 20-W output power, 6.5-dB gain, and 40% power-added efficiency (PAE) at 7.5 GHz was reported and a high-efficiency HBT monolithic-microwave integrated-circuit (MMIC) linear power amplifier for personal communication application has also been demonstrated, where the output power was 21 dBm and PAE was 35% [3], [4]. An ultra-low dc-power HBT low-noise amplifier (LNA) was also reported to have an IP3 level of 22 dBm with 20-mW dc-power consumption at 2 GHz [5].

In spite of the excellent experimental results, the mechanisms responsible for the good linear behavior of AlGaAs/GaAs HBT's have not been clearly understood. Maas attributed the good IM performance of HBT's to the exact cancellation of the IM currents between the emitter–base dynamic resistance r_{je} and capacitance C_{BE} [6]. According to [7], the IM currents generated by r_{je} and C_{BE}, and the IM currents generated by the total emitter–base current and the total base–collector current all partially cancel. Wang *et al*. [8] have reported that the feedback effect of the emitter resistance R_{E} and the base resistance R_{B} linearized the HBT output power and reduced the third-order IM distortion (IMD3). He also suggested that the C_{BC} nonlinearity caused deterioration of IMD3 performance. From these results, the mechanisms for the nonlinearity of HBT's are not clearly understood and should, therefore, be clarified. Furthermore, all the reported works used experimentally determined HBT models and could not provide design guidelines for an HBT structure optimized for good linearity.

To clearly understand the IM characteristics of the HBT and to find the optimized linear HBT structure, we have developed an analytical nonlinear HBT equivalent circuit model and computer program calculating IP3 based on Volterra-series analyses [9]–[12]. The simulation results have shown that the punchthrough collector is the best structure for a linearized HBT. Although IP3 does not depend on the emitter structure, it is appreciably affected by base and collector structures. Based on the simulation results, an optimized linear HBT structure has been proposed and its validity has been experimentally demonstrated.

The IM mechanism of the HBT has also been studied by investigating the cancellation effects of IM components generated by nonlinear elements. The output current distortion components generated by emitter–base current source and base–collector current source cancel each other almost exactly, resulting in high linearity. It is also shown that the base–collector capacitance is the key parameter determining the IP3 of an HBT. In Sections II and III, the device nonlinear model is discussed and simulation results are compared with two-tone test results on fabricated HBT's. In Section IV, cancellation mechanisms of HBT nonlinear components are discussed in detail.

II. Nonlinear HBT Model

The schematic HBT structure used for the analysis is shown in Fig. 1. In this figure, S_i, L_i, and W_i are the width, length, and thickness of the emitter, base, and collector, respectively

Manuscript received January 16, 1996; revised August 22, 1997. This work was supported in part by the Agency for Defense Development and Korean Telecommunication Company.

J. Lee was with Pohang University of Science and Technology (POSTECH), Pohang, Hyoja-dong, Kyung-pook, 790-784 Korea. He is now with Hyundai Electronics System IC Research and Development Laboratories, Ichon, Kyoungki-Do, 467-860 Korea.

W. Kim, Y. Kim, and B. Kim are with the Department of Electronic and Electrical Engineering and Microwave Application Research Center, Pohang University of Science and Technology (POSTECH), Pohang, 790-784 Korea.

T. Roh was with the Department of Electronic and Electrical Engineering and Microwave Application Research Center, Pohang University of Science and Technology (POSTECH), Pohang, 790-784 Korea. He is now with Samsung Electronics, Kumi, 730-350 Korea.

Publisher Item Identifier S 0018-9480(97)08239-2.

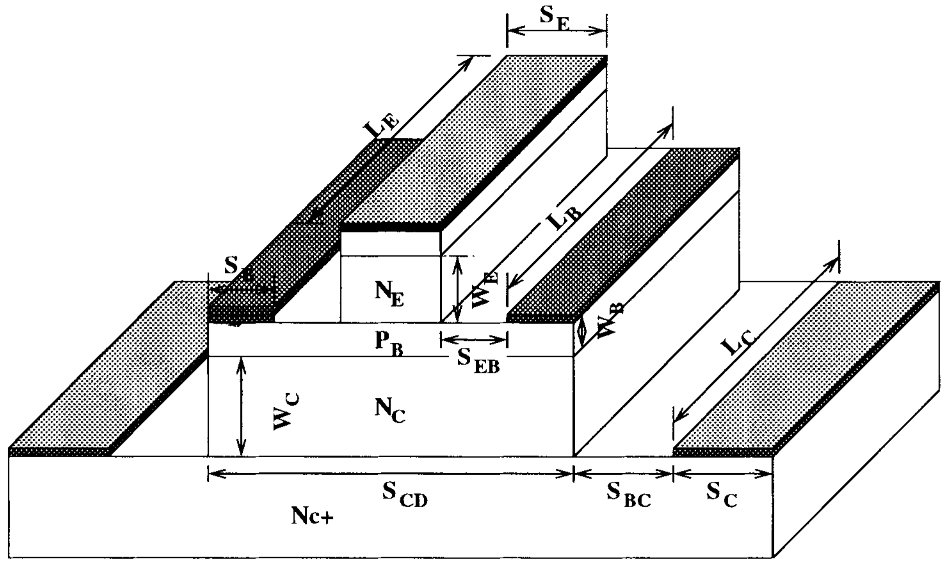

Fig. 1. Schematic structure of an HBT.

TABLE I
HBT MODEL PARAMETERS USED IN THE SIMULATION

Symbol	Value	Symbol	Value
ρ_{EC}	1×10^{-6} Ω·cm^2	$\varepsilon_{E,AlGaAs}$	1.09×10^{-12} F/cm
ρ_{BC}	3×10^{-6} Ω·cm^2	ε_B, ε_C	1.16×10^{-12} F/cm
ρ_{CC}	1×10^{-6} Ω·cm^2	ΔE_C	0.205 eV
L_E	20 μm	ΔE_V	0.109 eV
L_B	24 μm	N_{CD}	4.70×10^{17} cm^{-3}
L_C	24 μm	N_{VA}	7.0×10^{18} cm^{-3}
S_E	3 μm	m_n*	0.07 m_0
S_B	2 μm	m_p*	0.5 m_0
S_C	4 μm	τ_n, τ_p	2.0×10^{-9} sec
S_{EB}	0.2 μm	V_{TH}	0.0259 V
S_{BC}	2 μm	J_{RB}	4.0×10^{-12} A/cm^2
S_{CD}	7 μm	η_B	1.92

($i =$ E, B, and C). The doping concentrations of the emitter, base, and collector are $N_{\rm E}$, $P_{\rm B}$, and $N_{\rm C}$, respectively, and the distance between emitter and base, and base and collector are $S_{\rm EB}$ and $S_{\rm BC}$, respectively. The device model parameters used in the simulation are summarized in Table I [13]–[15]. All equivalent circuit parameter values are obtained as functions of the HBT structures.

Fig. 2 shows the HBT equivalent circuit with matching network used for the simulation. The simultaneously conjugate-matched input and output networks were designed from the calculated S-parameters of the equivalent circuit. In the figure, ohmic resistances $R_{\rm E}$, $R_{\rm B}$, $R_{\rm C}$, and output impedance r_o are linear components calculated from the HBT structure, while the base–emitter nonlinear current source $I_{\rm e}$, the base–collector nonlinear current source $I_{\rm c}$, the base–emitter capacitance $C_{\rm BE}$, and the base–collector capacitance $C_{\rm BC}$ are nonlinear elements that vary with applied bias. The ohmic resistances of the HBT

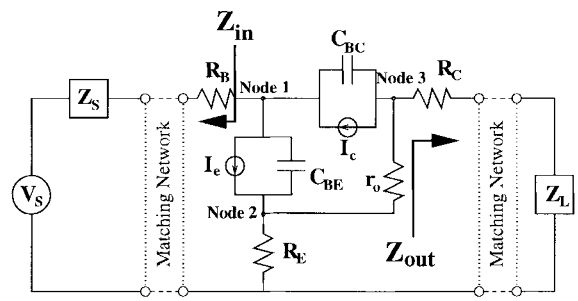

Fig. 2. Nonlinear HBT equivalent circuit model with matching networks.

($R_{\rm E}$, $R_{\rm B}$, $R_{\rm C}$) are calculated from the following equations:

$$R_{\rm E} = \frac{\rho_{\rm EC}}{S_{\rm E}L_{\rm E}} + \frac{1}{q\mu_{nE}N_{\rm E}}\frac{W_{\rm E}}{S_{\rm E}L_{\rm E}} \tag{1}$$

$$R_{\rm B} = \frac{R_{\rm SB}S_{\rm E}}{12L_{\rm E}} + \frac{R_{\rm SB}S_{\rm EB}}{2L_{\rm E}} + \frac{\sqrt{\rho_{\rm BC}R_{\rm SB}}}{2L_{\rm B}} \cdot \coth S_{\rm B}\sqrt{\frac{R_{\rm SB}}{\rho_{\rm BC}}} \tag{2}$$

$$R_{\rm C} = \frac{R_{\rm SC}S_{\rm CD}}{12L_{\rm C}} + \frac{\sqrt{\rho_{\rm CC}R_{\rm SC}}}{2L_{\rm C}} \cdot \coth S_{\rm C}\sqrt{\frac{R_{\rm SC}}{\rho_{\rm CC}}} + \frac{R_{SC}S_{\rm BC}}{2L_{\rm C}} + \frac{1}{q\mu_{n\rm C}N_{\rm C}}\frac{W_{\rm C}}{S_{\rm CD}L_{\rm C}} \tag{3}$$

where $\rho_{\rm EC}$, $\rho_{\rm BC}$, and $\rho_{\rm CC}$ are the specific contact resistivities of emitter, base, and collector, respectively, while $R_{\rm SB}$ and $R_{\rm SC}$ are the sheet resistances of the base and sub-collector layer, respectively. All the other parameters have their nominal meanings. The output impedance r_o is given by

$$r_o = \frac{V_{\rm A}}{I_{\rm C}} = \frac{1}{I_{\rm C}}\frac{\eta_{\rm C}Q_{\rm B}}{\eta_{\rm E}C_{\rm BC}} \tag{4}$$

where $V_{\rm A}$ is early voltage, $Q_{\rm B}$ is total majority carrier charge in the base, and $\eta_{\rm E}$ and $\eta_{\rm C}$ are the ideality factors of the emitter and collector junctions, respectively.

The nonlinear elements can be expanded in terms of the node voltages. We considered only up to the third-order expansion coefficients in the Volterra-series to calculate IP3. The stored charge at base–emitter junction $Q_{\rm BE}$ is composed of depletion and diffusion charges and is given by

$$Q_{\rm be} = \sqrt{2\epsilon q N_{\rm E}}\left(\sqrt{V_{\rm bi}} - \sqrt{V_{\rm bi} - V_{\rm be}}\right)A_{\rm E} + I_{\rm e}\tau_{\rm B} \qquad (5)$$

where $\tau_{\rm B}$ is the base transit time. In the normal operating region, the diffusion capacitance dominates and the effect of the possible error in the depletion capacitance is acceptable. The nonlinear current source $I_{\rm e}$ is given by [15] and [16] as follows:

$$I_{\rm e} = I_{\rm SE}\left[\exp\left(\frac{V_{\rm be}}{V_{\rm TH}}\right) - 1\right] + I_{\rm RE}\left[\exp\left(\frac{V_{\rm be}}{\eta_{\rm B} V_{\rm TH}}\right) - 1\right] \qquad (6)$$

where $I_{\rm SE}$ represents the injection current and $I_{\rm RE}$ accounts for the recombination current. Since these parameters depend only on $V_{\rm be}$, they can be expanded as

$$q_{\rm be} = c_{\rm e1}v_{\rm be} + c_{\rm e2}v_{\rm be}^2 + c_{\rm e3}v_{\rm be}^3 \qquad (7)$$

$$i_{\rm e} = k_{\rm e1}v_{\rm be} + k_{\rm e2}v_{\rm be}^2 + k_{\rm e3}v_{\rm be}^3 \qquad (8)$$

where the $q_{\rm be}$, $v_{\rm be}$, and $i_{\rm e}$ are the small-signal components of $Q_{\rm be}$, $V_{\rm be}$, and $I_{\rm e}$, respectively. The coefficients in the above equations are given by the Taylor-series expansion of $Q_{\rm be}$ and $I_{\rm e}$ with respect to $V_{\rm be}$.

The nonlinear base–collector capacitance $C_{\rm BC}$ was modeled as

$$W_d = \sqrt{\frac{2\epsilon(V_{\rm bi} + V_{\rm cb})}{qN_{\rm C}}} \qquad (9)$$

$$C_{\rm BC} = \frac{\epsilon A_{\rm C}}{W_d}, \qquad \text{for } W_d \le W_{\rm C}$$

$$C_{\rm BC} = \frac{\epsilon A_{\rm C}}{W_{\rm C}}, \qquad \text{for } W_d > W_{\rm C} \qquad (10)$$

where $A_{\rm C}$ is the collector area. The stored charge at the base–collector junction $Q_{\rm bc}$ is dependent only on $V_{\rm cb}$, so the small-signal component $q_{\rm bc}$ can be expanded as follows:

$$q_{\rm bc} = c_{\rm c1}v_{\rm cb} + c_{\rm c2}v_{\rm cb}^2 + c_{\rm c3}v_{\rm cb}^3 \qquad (11)$$

where the coefficient c_{ci} is the Taylor-series expansion of $Q_{\rm bc}$ with respect to $V_{\rm cb}$. The small-signal current can be obtained by taking the time derivative of $q_{\rm bc}$. The nonlinear current source at the base–collector junction $I_{\rm c}$ is given by

$$I_{\rm c} = \alpha I_{\rm e}. \qquad (12)$$

The common base current gain α can be written as

$$\alpha = \alpha_0 \frac{\exp(-j\omega\tau)}{1 + j\dfrac{\omega}{\omega_\alpha}} \qquad (13)$$

where τ and ω_α are the base–collector transit time and α-cutoff frequency, respectively. The dc current gain α_o was modeled as in [15]–[18]. Since $I_{\rm e}$ and α_o depend on only $V_{\rm be}$, the small-signal component of the collector current can be represented as follows:

$$i_{\rm c} = k_{\rm c1}v_{\rm be} + k_{\rm c2}v_{\rm be}^2 + k_{\rm c3}v_{\rm be}^3 \qquad (14)$$

where k_{ci} is the Taylor-series expansion of $I_{\rm c}$ with respect to $V_{\rm be}$. By using all the above expansion coefficients, the node equations in the HBT equivalent circuit of Fig. 2. can be found as

$$\frac{v_s - v_1}{Z_{\rm in}} = \sum_{i=1}^{3}(k_{ei} - k_{ci} + j\omega c_{ei})v_{12}^i - \sum_{i=1}^{3} j\omega c_{ei} v_{31}^i$$

$$0 = \frac{v_2}{R_{\rm E}} - \sum_{i=1}^{3}(k_{ei} + j\omega c_{ei})v_{12}^i + \frac{v_{23}}{r_o}$$

$$0 = \frac{v_3}{Z_{\rm out}} + \sum_{i=1}^{3}(k_{ci}v_{12}^i + j\omega c_{ci}v_{31}^i) + \frac{v_{32}}{r_o} \qquad (15)$$

where $v_{ij} = v_i - v_j$, and $Z_{\rm in}$ and $Z_{\rm out}$ are indicated in Fig. 2. The ith-order transfer function is obtained directly from the above node equations for each $i(= 1, 2, 3)$. The linear components $Z_{\rm in}$, $Z_{\rm out}$, $R_{\rm E}$, $R_{\rm B}$, $R_{\rm C}$ and r_o are included only in the first-order transfer function.

III. Design of the Linearized HBT's

A. Simulation Results

To find out the optimum HBT structures maximizing IP3, we have investigated the IP3 dependence of HBT structures under various bias conditions ($I_{\rm CE}$, $V_{\rm CE}$). A two-tone simulation was performed as a function of $N_{\rm E}$, $P_{\rm B}$, $N_{\rm C}$, $W_{\rm E}$, $W_{\rm B}$, and $W_{\rm C}$ at frequencies $f_1 = 10$ GHz and $f_2 = f_1 + \Delta f$, where $\Delta f = 10$ MHz. We applied simultaneous conjugate matching conditions to the simulation because power matching cannot be implemented for the analysis. The simulation results are shown in Fig. 3. under bias condition of $V_{\rm CE} = 3$ V and $I_{\rm C} = 24$ mA ($J_{\rm C} = 4 \times 10^4$ A/cm^2).

Fig. 3(a) shows IP3 dependence on the collector doping and thickness. The base doping and thickness are 2×10^{19} cm^{-3} and 0.1 μm, respectively. It should be noted that IP3 is very high when the collector is fully depleted. The IP3 of punchthrough collector devices is about 10 dB higher than that of the normal device. The discontinuities in the IP3 lines due to the transition from the collector punchthrough region to the nonpunchthrough region for the given bias. We have observed similar behavior at different bias conditions. The base-structure dependency on IP3 performance is shown in Fig. 3(b). The collector doping is 2×10^{16} cm^{-3} and the collector thicknesses is 1.0 μm. As shown in Fig. 3(b), IP3 weakly depends on the base thickness, but it is rather strongly dependent on base doping. For $W_{\rm B} = 0.1\,\mu$m, it improves by about 3 dB as the base doping decreases from 3×10^{19} cm^{-3} to 1×10^{19}cm^{-3}. In the widely used range of base doping and thickness, IP3 of the chosen device is between 24–28 dBm. Fig. 3(c) shows IP3 dependence on the emitter doping. The base and collector dopings are 2×10^{19} cm^{-3} and 2×10^{16} cm^{-3}, respectively, and the emitter, base, and collector

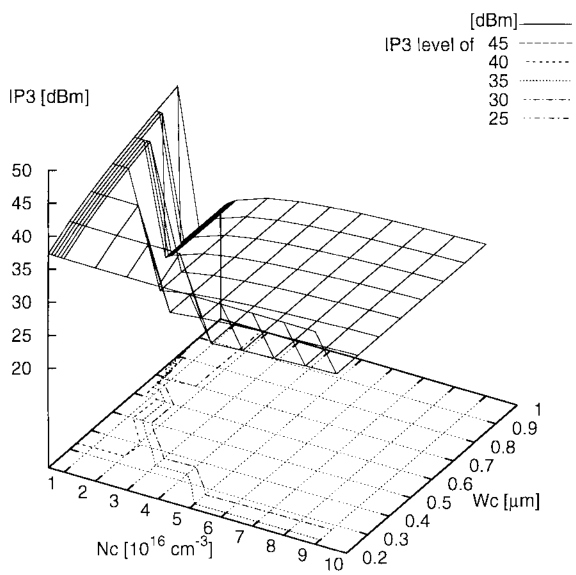

(a)

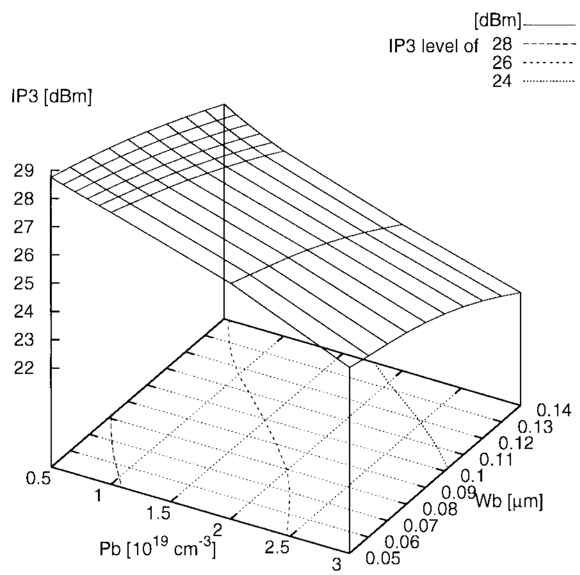

(b)

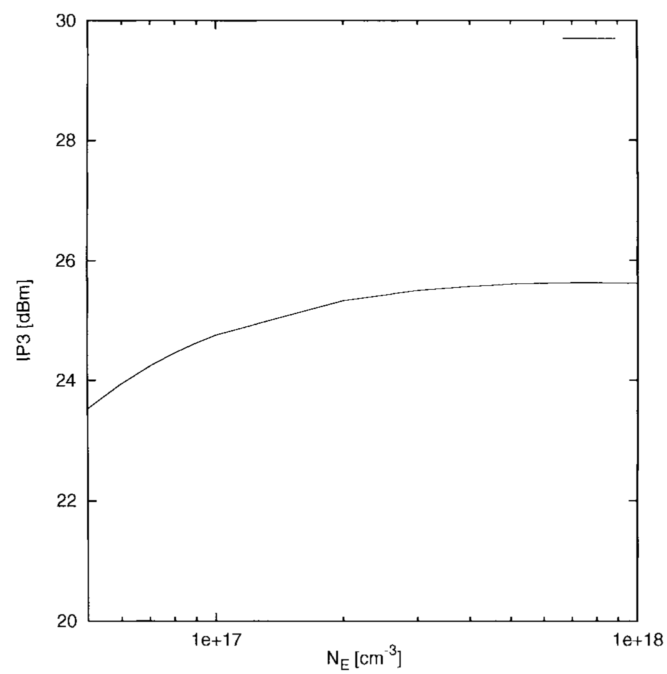

(c)

Fig. 3. HBT structure effects on the IP3 performance. (a) IP3 dependence on the collector parameters ($N_{\mathrm{E}} = 2 \times 10^{17}$ cm^{-3}, $P_{\mathrm{B}} = 2 \times 10^{19}$ cm^{-3}, $W_{\mathrm{E}} = 0.2\,\mu$m, $W_{\mathrm{B}} = 0.1\,\mu$m). (b) IP3 dependence on the base parameters ($N_{\mathrm{E}} = 2 \times 10^{17}$ cm^{-3}, $N_{\mathrm{C}} = 2 \times 10^{16}$ cm^{-3}, $W_{\mathrm{E}} = 0.2\,\mu$m, $W_{\mathrm{C}} = 1.0\,\mu$m). (c) IP3 dependence on the emitter doping ($P_{\mathrm{B}} = 2 \times 10^{19}$ cm^{-3}, $N_{\mathrm{C}} = 2 \times 10^{16}$ cm^{-3}, $W_{\mathrm{E}} = 0.2\,\mu$m, $W_{\mathrm{B}} = 0.1\,\mu$m, $W_{\mathrm{C}} = 1.0\,\mu$m).

thicknesses are 0.2, 0.1, and 1.0 μm, respectively. Thus, IP3 is insensitive to the emitter doping, in agreement with the results of Wang *et al.* [8].

From the above simulation results, IP3 performance of the HBT does not strongly depend on the emitter parameters, while it is appreciably dependent on base and collector parameters. In particular, the device linearity is remarkably improved in the punchthrough collector structure. We have utilized the simulation results in choosing three HBT structures for our experiment. HBT2 is a typical power-structure HBT with $W_{\mathrm{B}} = 0.1\,\mu$m and $W_{\mathrm{C}} = 1.0\,\mu$m. To verify the base-structure effect on IP3 performance, the base thickness of HBT3 was chosen to be 0.14 μm. HBT1 is the punchthrough collector structure HBT with $W_{\mathrm{C}} = 0.4\,\mu$m. Since IP3 is not sensitive to emitter parameters, all three HBT's have the same emitter doping (2×10^{17} cm^{-3}) and thickness (0.2 μm). The doping concentrations of the base and collector are 2×10^{19} cm^{-3} and 2×10^{16} cm^{-3}, respectively.

Fig. 4(a) and (b) show IP3 performances of HBT1 and HBT2 as functions of the applied biases. We can see that IP3 is more sensitive to the collector-bias voltage than to the collector-bias current. It suggests that the base–collector capacitance C_{BC} is the key element determining IP3 performance of HBT. Note that the IP3 value of HBT1 is remarkably improved

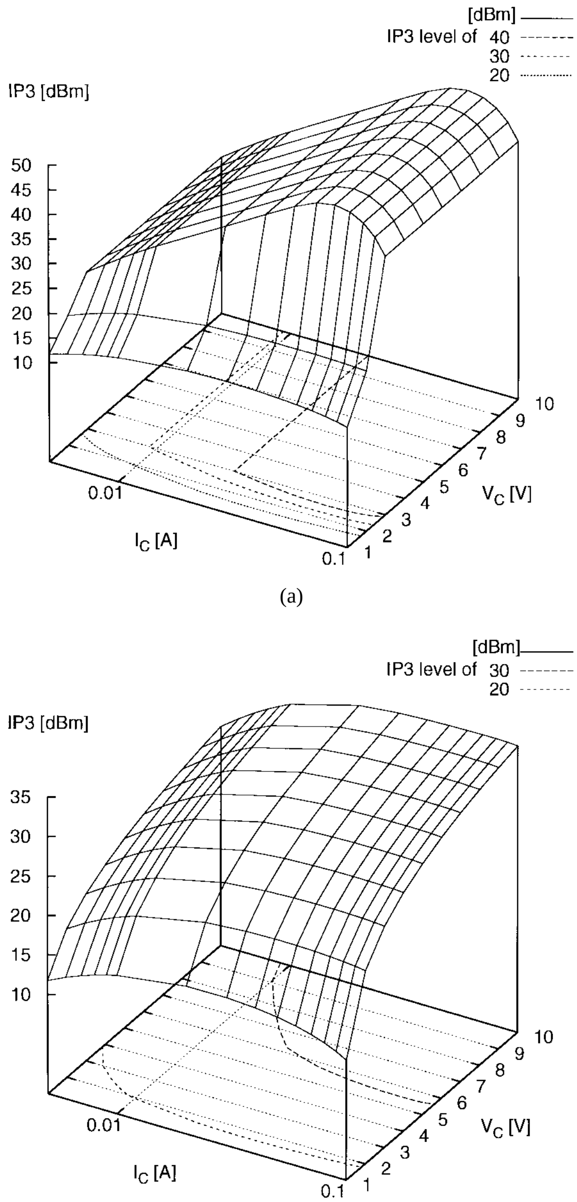

(a)

(b)

Fig. 4. Simulated IP3 level of HBT's as a function of applied bias. (a) HBT1. (b) HBT2.

at punchthrough bias condition. It has the same IP3 value as HBT2 when the collector is not fully depleted. HBT3 showed similar IP3 performance to HBT2. However, its IP3 level was slightly lower than that of HBT2 at the same bias voltage.

B. Two-Tone Test Results

We have fabricated AlGaAs/GaAs HBT's using the self-aligned base metal (SABM) process technique. The epilayer structures designed from the above simulation were used. Our HBT structure, process, and main dc/RF performances were reported in detail elsewhere [19].

The two-tone test has been performed to characterize the linearity of the three HBT's. An HP8350B Sweep Oscillator was used as an RF source and FOCUS1808 Programmable Tuner was used to match the devices. The input frequencies of two RF sources were selected at 10 and 10.01 GHz. The

TABLE II
TWO-TONE POWER-TEST RESULTS OF THE HBT's (I_c = 15 MA AND V_{CE} = 3 V)

	#19294 HBT	#19394 HBT	#19894 HBT
P_{1dB} [dBm]	10.3	9.5	10.1
Power Gain [dB]	7.2	7.3	7.6
$Efficiency_{1dB}$ [%]	18	14	17
$IMD3_{1dB}$ [dBc]	-36	-33	-32
IP3 [dBm]	31	28	28
LFOM	28	14	14
I_b [mA]	0.44	0.47	1.15
Γ_S	0.199 ∠-17.5	0.031 ∠-77.2	0.203 ∠-45.0
Γ_L	0.292 ∠-89.0	0.423 ∠-124.6	0.426 ∠-109.7
$IP3_{SIM}$ [dBm]	35	25	25

HBT's was biased with an HP6626A dc Power Supply and output power level was measured using an HP8562A Spectrum Analyzer. The characterization system was automatically controlled by the computer connected to the measurement setup. The IP3 level of the devices were obtained by extrapolating $P1_{\mathrm{out}}$ and $P3_{\mathrm{out}}$ powers at a linear gain region.

Fig. 5(a)–(c) shows the two-tone test results of the devices under the same bias condition of $I_C = 15$ mA and $V_{CE} = 3$ V. The main results have been summarized in Table II. As shown in the figure, two HBT's with normal collectors exhibit similar performance. At the 1-dB gain compression point, the IMD3 of the HBT2 is −33 dBc with output power of 9.5 dBm and that of HBT3 is −32 dBc with output power of 10.1 dBm. The IP3 level of the devices extrapolated from the linear gain region is 28 dBm, which corresponds to linearity figure of merit (LFOM = IP3/P_{dc}) of 14 [8]. For HBT1 with punchthrough collector, IMD3 is −36 dBc with output power of 10.1 dBm. The IP3 value of the device is 31 dBm, which corresponds to an LFOM of 28 and is higher than that of HBT2 or HBT3 by 3 dB. Compared with the simulation results, the measured IP3 of the normal collector HBT is higher by 3 dB, while that of HBT1 is lower by 4 dB. The main cause of the differences between experimental and simulation results can be attributed to the fact that the simulation was performed at the small-signal gain matching condition. However, it is clear that the punchthrough collector device exhibits better IP3 performance than the normal collector device.

IV. CANCELLATION MECHANISM OF HBT NONLINEAR COMPONENTS

As mentioned earlier, it is not clear why HBT's exhibit good linearity in spite of the presence of strong nonlinear components. To clearly understand the nonlinear mechanism of HBT's, we have investigated the contribution of the nonlinear elements to IP3. The typical power HBT structure (HBT2) was chosen for the simulation. First, the effects of each nonlinear element of an HBT have been studied by artificially linearizing the nonlinear element under consideration. Next, the cancellation mechanisms among the nonlinear components were investigated by considering only two nonlinear elements at a time.

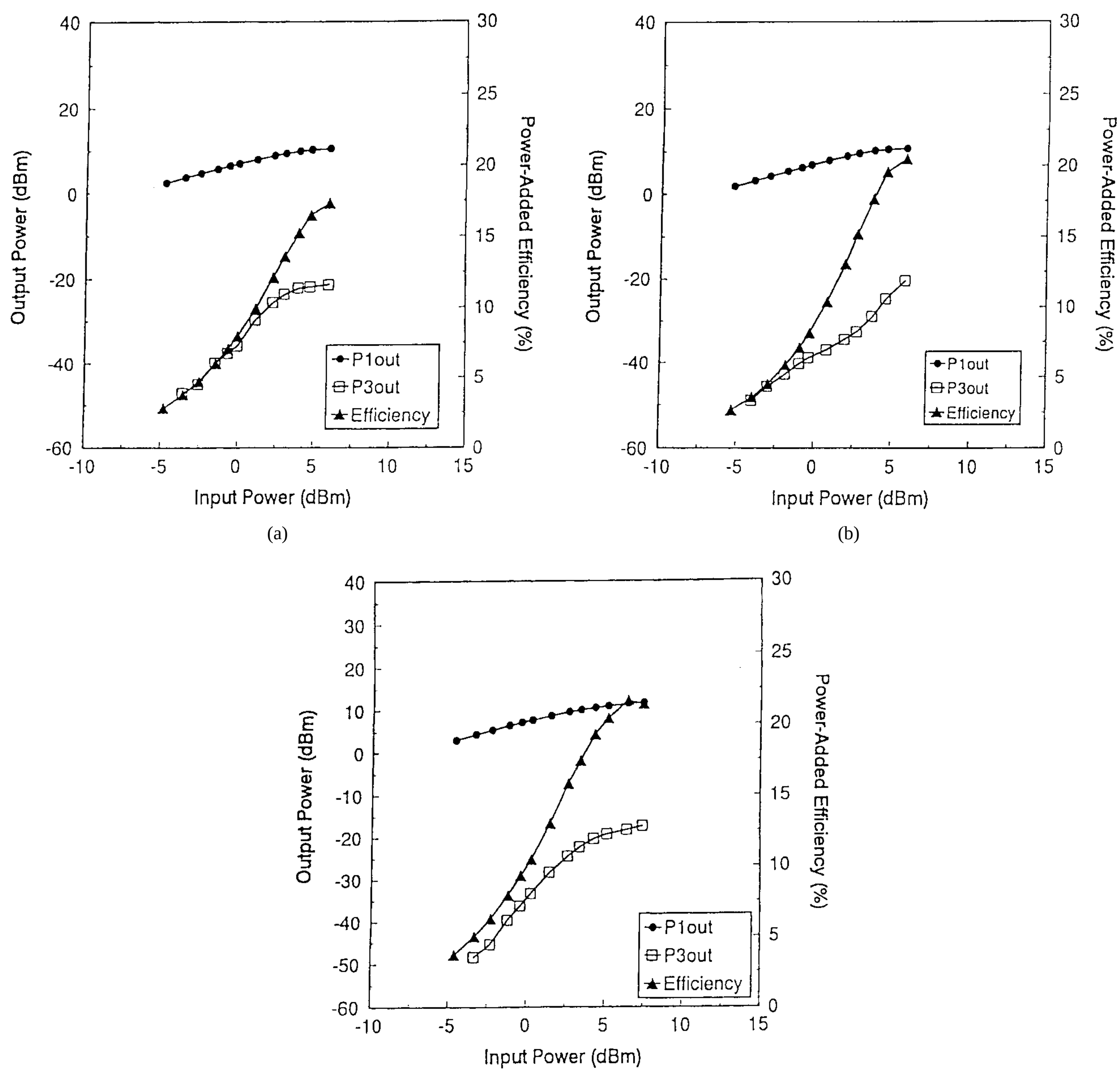

Fig. 5. Measured power-added efficiency, fundamental, and third-order output powers of HBT's as a function of input power ($I_C = 15$ mA and $V_{CE} = 3$ V). (a) HBT1. (b) HBT2. (c) HBT3.

Fig. 6(a) and (b) shows the IP3 performance of the HBT when the base–emitter nonlinear current source I_e or the collector current source I_c is substituted by a linear element. Compared with the normal HBT with all nonlinear elements, the IP3 level falls off by a large amount in the low collector-bias region [see Fig. 4(b)]. In these cases, IP3 depends on the collector current as well as the collector-bias voltage. However, as shown in the Fig. 6(c), IP3 is improved by more than 13 dB by eliminating the nonlinearity of base–collector capacitance C_{BC}. Note that IP3 is more sensitive to the collector current than the collector voltage because C_{BC} nonlinearity originating from the collector-bias voltage is eliminated. When the third-order component of the nonlinear current generated by C_{BE} source was removed by treating it as a linear element, the IP3 level of HBT was reduced by less than 1 dB from that of normal HBT. This result indicates that C_{BE} is not a key element in determining IP3 level, in agreement with the previous results of Section III.

Fig. 6(d) shows IP3 performance when both I_e and I_c are treated as linear elements and only C_{BE} and C_{BC} are operated as nonlinear sources. Note that their IP3 performances are quite similar to the result of the normal HBT with all nonlinear sources except for the very low collector-bias current region. As previously pointed out, IP3 appreciably falls off if one of the third-order nonlinear currents generated by the I_e and I_c sources was eliminated. This indicates that the harmonic components generated by two nonlinear current sources of I_e and I_c cancel each other almost exactly, resulting in high linearity. We have also investigated the cancellation effects of other components, but there were no other significant cancellation effects between IM currents.

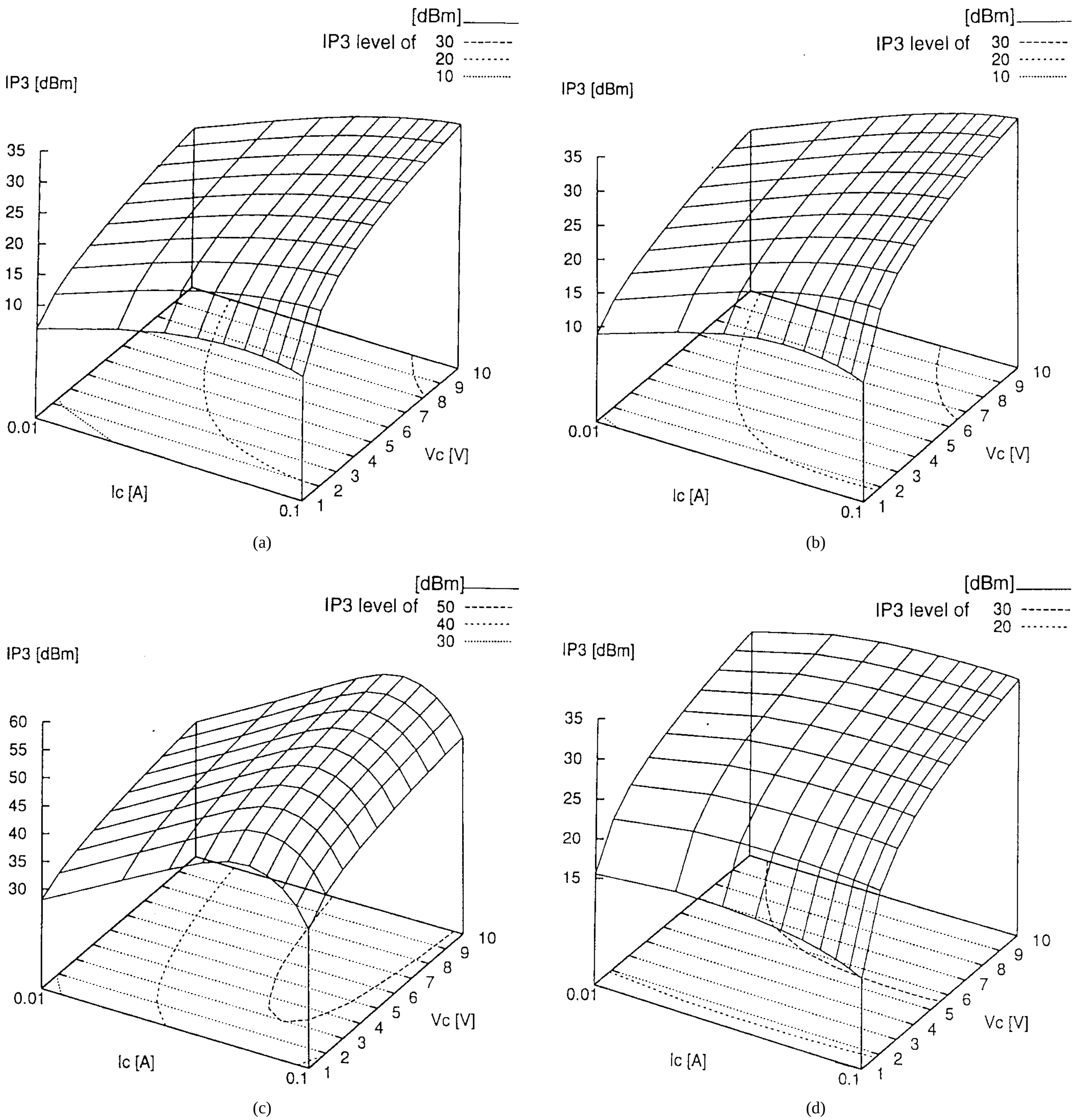

Fig. 6. IP3 level of HBT2. (a) IP3 level of HBT with linearized I_e. (b) IP3 level of HBT with linearized I_c. (c) IP3 level of HBT with linearized C_{BC}. (d) IP3 level of HBT with linearized I_e and I_c.

V. Conclusion

An analytical nonlinear HBT equivalent circuit model and computer program for calculating IP3 have been developed to understand the IM characteristics of HBT's and to find the optimized linear HBT structure. The simulation results have shown that IP3 performance of the HBT does not strongly depend on the emitter parameters, while the performance is appreciably dependent on base and collector parameters. In particular, the device linearity has been dramatically improved using the punchthrough collector structure. The collector punchthrough device exhibited an IP3 level of 31 dBm, which was 3 dB higher than that of normal collector HBT's. Based on simulation results, we have proposed an optimized linear HBT structure. The investigation of the cancellation mechanisms among the nonlinear components has shown that the harmonic components generated by the emitter–base current source and base–collector current source cancel each other out almost exactly, resulting in high linearity of the HBT. C_{BE} does not affect the HBT linearity, but C_{BC} is a very strong nonlinear source and should be linearized using the punchthrough collector structure for reduced distortion.

REFERENCES

[1] B. L. Nelson *et al.*, "High-linearity, low dc power GaAs HBT broadband amplifiers to 11 GHz," in *1989 IEEE GaAs IC Symp. Dig.*, San Diego, CA, Oct. 1989, pp. 79–82.

[2] M. E. Kim *et al.*, "12–40 GHz low harmonic distortion and phase noise performance of GaAs HBT's," in *1988 IEEE GaAs IC Symp. Dig.*, Nashville, TN, Nov. 1988, pp. 117–120.

[3] P. K. Ikalainen, S.-K. Fan, and M. A. Khatibzadeh, "20 W linear, high efficiency internally matched HBT at 7.5 GHz," in *IEEE MTT Symp. Dig.*, San Diego, CA, May 1994, pp. 679–682

[4] T. Yoshimasu, N. Tanba, and S. Hara, "High efficiency HBT MMIC linear power amplifier for L-band personal communications systems," *IEEE Microwave Guided Wave Lett.*, vol. 4, pp. 65–67, Mar. 1994.

[5] K. W. Kobayashi, A. K. Oki, L. T. Tran, and D. C. Streit, "Ultra-low dc power GaAs HBT S-band low noise amplifiers," in *IEEE Microwave Millimeter-Wave Monolithic Circuits Symp. Dig.*, Orlando, FL, May 1995, pp 73–76.

[6] S. A. Maas, B. L. Nelson, and D. L. Tait, "Intermodulation in HBT's," *IEEE Trans. Microwave Theory Tech.*, vol. 40, pp. 442–448, Mar. 1992.

[7] A. Samelis and D. Pavlidis, "Mechanisms determining third-order intermodulation distortion in AlGaAs/GaAs HBT's," *IEEE Trans. Microwave Theory Tech.*, vol. 40, pp. 2374–2380, Dec. 1992.

[8] N. L. Wang, W. J. Ho, and J. A. Higgins, "AlGaAs/GaAs HBT linearity characteristics," *IEEE Trans. Microwave Theory Tech.*, vol. 42, pp. 1845–1850, Oct. 1994.

[9] S. Narayanan, "Transistor distortion analysis using Volterra-series representation," *Bell Syst. Tech. J.*, vol. 46, pp. 991–1024, May–June 1967.

[10] A. A. Saleh, "Matrix analysis of mildly nonlinear, multiple-input, multiple-output systems with memory," *Bell Syst. Tech. J.*, vol. 60, pp. 2221–2243, Nov. 1982.

[11] S. Narayanan and H. C. Poon, "An analysis of distortion in bipolar transistors using integral charge control model and Volterra-series," *IEEE Trans. Circuit Theory*, vol. CT-20, pp. 341–351, Apr. 1973.

[12] H. C. Poon, "Implication of transistor frequency dependence on intermodulation distortion," *IEEE Trans. Electron Devices*, vol. ED-21, pp. 110–112, Jan. 1974.

[13] B. R. Ryum and I. M. Abdel-Motaleb, "A Gummel–Poon model for abrupt and graded HBT's," *Solid State Electron.*, vol. 33, no. 7, pp. 869–880, July 1992.

[14] H. C. Casey, Jr. and M. B. Panish, *Heterostructure Lasers.* New York: Academic, 1978.

[15] A. A. Grinberg, M. S. Shur, R. J. Fischer, and H. Morkoc, "An investigation of the effect of graded layers and tunneling on the performance of AlGaAs/GaAs HBT's," *IEEE Trans. Electron Devices*, vol. ED-31, pp. 1758–1765, Dec. 1984.

[16] H.-H. Lin and S.-C. Lee, "Super-gain AlGaAs/GaAs HBT's using an emitter edge-thinning design," *Appl. Phys. Lett.*, vol. 47, no. 8, pp. 839–841, Oct. 1985.

[17] J. J. Liou, F. A. Lindholm, and D. C. Malocha, "Forward-voltage capacitance of heterojunction space-charge regions," *J. Appl. Phys.*, vol. 63, no. 10, pp. 5015–5022, May 1988.

[18] N. Chand and H. Morkoc, "Doping effects and compositional grading in $Al_xGa_{1-x}As$/GaAs HBT's," *IEEE Trans. Electron Devices*, vol. ED-32, pp. 1064–1069, June 1985.

[19] J. Lee, Y. Suh, J. Shin, B. Kim, Y. L. Jung, H. C. Seo, W. Jung, and D. S. Ma, "Experimental study of emitter size effects of microwave AlGaAs/GaAs HBT's," in *Proc. ICVC'95*, Seoul, Korea, Oct. 1995, pp. 361–363.

Joonwoo Lee (S'93–A'95–M'96) was born in Kangwon-Do, Korea, in 1963. He received the B.S. degree in electronics engineering from Seoul National University, Seoul, Korea, in 1990, and the M.S. and Ph.D. degrees in electronic and electrical engineering from Pohang University of Science and Technology, Pohang, Korea, in 1992 and 1996, respectively.

In 1996, he joined Hyundai Electronics System IC Research and Development Laboratories, Ichon, Kyoungki-Do, Korea, where he is currently developing photonic and high-speed electronic devices such as DFB laser diodes, photodetectors, and HBT's. His research interests include fabrication, modeling, and characterization of InP- and GaAs-based devices and their integration into optoelectronic and microwave-integrated circuits.

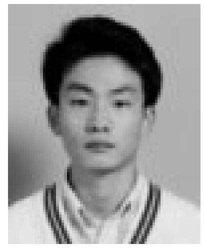

Woonyun Kim (S'95) was born in Seoul, Korea, in 1970. He received the B.S. and M.S. degrees in electronic and electrical engineering from Pohang University of Science and Technology, Pohang, Korea, in 1994 and 1996, respectively, and is currently working toward the Ph.D. degree.

His research activities are concentrated in the design and fabrication of AlGaAs/GaAs linear power HBT's and MMIC's.

Youngsik Kim (S'97) received the B.S. and M.S. degrees from Pohang University of Science and Technology, Pohang, Korea, in 1993 and 1995, respectively, and is currently working toward the Ph.D. degree.

His research interests are active device modeling, linear power amplifier design, and developing a nonlinear circuit simulator.

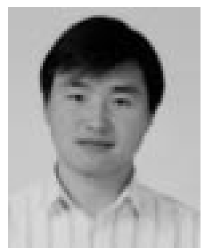

Taemoon Rho (M'97) was born in Pusan, Korea, in 1968. He received the M.S. degree in electronics and the Ph.D. degree from Pohang University of Science and Technology, Pohang, Korea, in 1993 and 1997, respectively.

His research activities are concentrated in GaAs MESFET modeling and linear power amplifier design. He is currently with Samsung Electronics, Kumi, Korea, where he is working on the PCS handset RF system.

Bumman Kim (S'77–M'78) received the Ph.D. degree in electrical engineering from Carnegie-Mellon University, Pittsburgh, PA, in 1979.

From 1978 to 1981, he was engaged in fiber-optic component research at GTE Laboratories Inc. In 1981, he joined the Central Research Laboratories of Texas Instruments, Inc., where he was involved in development of GaAs power FET's and monolithic microwave integrated circuits. He has developed a large-signal model of a power FET, dual-gate FET's for gain control, and high-power distributed amplifiers, and various millimeter-wave MMIC's. In 1989, he joined Pohang University of Science and Technology, Pohang, Korea, where he is a Professor in the Electronic and Electrical Engineering Department, and Director of the Microwave Application Research Center, working on device and circuit technology for MMIC's. He has published over 100 technical papers in this area.

Dr. Kim is a member of the Korean Academy of Science and Technology.